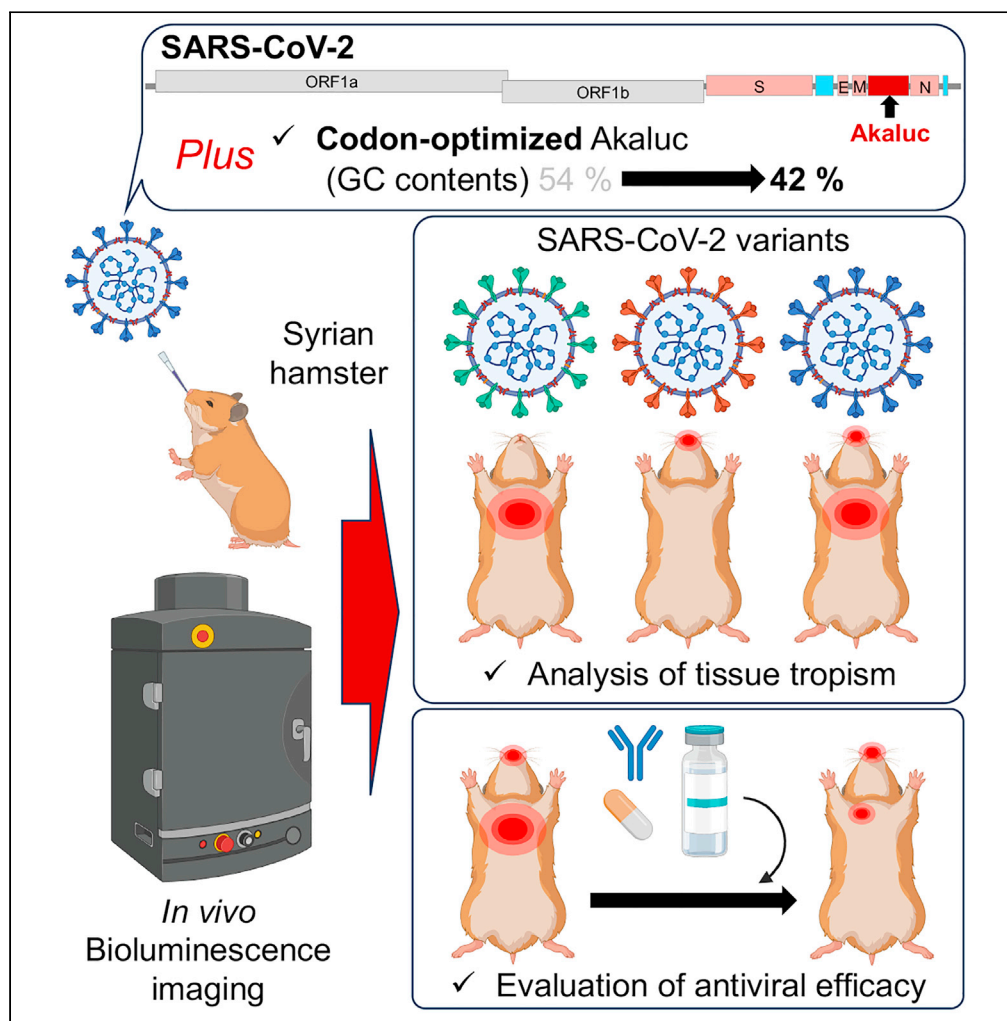


Article

Akaluc bioluminescence offers superior sensitivity to track *in vivo* dynamics of SARS-CoV-2 infection

Tomokazu
Tamura, Hayato
Ito, Shiho Torii, ...,
Satoshi Iwano,
Shinya Tanaka,
Takasuke Fukuhara

s.iwano0326@gmail.com (S.I.)
tanaka@med.hokudai.ac.jp
(S.T.)
fukut@pop.med.hokudai.ac.jp
(T.F.)

Highlights

The codon-optimizing
Akaluc can be successfully
accommodated in SARS-
CoV-2 genome

AkaBLI enables
spatiotemporal monitoring
of SARS-CoV-2 spread in
hamsters

AkaBLI is useful for
analyzing viral tissue
tropism and antiviral
efficacy

Tamura et al., iScience 27,
109647
May 17, 2024 © 2024 The
Authors. Published by Elsevier
Inc.
[https://doi.org/10.1016/
j.isci.2024.109647](https://doi.org/10.1016/j.isci.2024.109647)

Article

Akaluc bioluminescence offers superior sensitivity to track *in vivo* dynamics of SARS-CoV-2 infection

Tomokazu Tamura,^{1,2,3,19} Hayato Ito,^{1,19} Shiho Torii,^{4,19,20} Lei Wang,^{5,6,19} Rigel Suzuki,^{1,2} Shuhei Tsujino,¹ Akifumi Kamiyama,¹ Yoshitaka Oda,⁵ Masumi Tsuda,^{5,6} Yuhei Morioka,^{1,4} Saori Suzuki,^{1,2} Kotaro Shirakawa,⁷ Kei Sato,^{8,9,10,11,12,13,14} Kumiko Yoshimatsu,¹⁵ Yoshiharu Matsuura,^{4,16} Satoshi Iwano,^{17,*} Shinya Tanaka,^{5,6,*} and Takasuke Fukuhara^{1,2,3,4,18,21,*}

SUMMARY

Monitoring *in vivo* viral dynamics can improve our understanding of pathogenicity and tissue tropism. Because the gene size of RNA viruses is typically small, NanoLuc is the primary choice for accommodation within viral genome. However, NanoLuc/Furimazine and also the conventional firefly luciferase/D-luciferin are known to exhibit relatively low tissue permeability and thus less sensitivity for visualization of deep tissue including lungs. Here, we demonstrated *in vivo* sufficient visualization of severe acute respiratory syndrome coronavirus 2 (SARS-CoV-2) infection using the pair of a codon-optimized Akaluc and AkaLumine. We engineered the codon-optimized Akaluc gene possessing the similar GC ratio of SARS-CoV-2. Using the SARS-CoV-2 recombinants carrying the codon-optimized Akaluc, we visualized *in vivo* infection of respiratory organs, including the tissue-specific differences associated with particular variants. Additionally, we could evaluate the efficacy of antivirals by monitoring changes in Akaluc signals. Overall, we offer an effective technology for monitoring viral dynamics in live animals.

INTRODUCTION

Since the discovery of North American firefly luciferase (FLuc), bioluminescence has become a powerful tool¹ for *in vivo* studies of gene regulation, particularly bioluminescence imaging (BLI), which enables spatiotemporal monitoring of live animals. BLI has been utilized to monitor transgene expression, tumor growth, metastasis, and progression of infection.² The key to this technology is to find out good combination of the enzyme (luciferase) and substrates (luciferins) for shedding sufficient light. Luciferase-luciferin pairs have been discovered across diverse phyla, and when the correct pair of luciferase/luciferin are introduced into cells, these components can act as biological flashlights. FLuc and D-luciferin was the first enzyme-substrate combination for which bioluminescent signals could be measured in mice.³ Of the approximately 30 naturally occurring bioluminescence systems that have been discovered,⁴ currently, the pair of FLuc/D-luciferin is commonly used in small animals; the FLuc/D-luciferin produces longer wavelength (600 nm) showing more easily transmitted through tissue compared to other enzymes. The substrate D-luciferin is relatively stable *in vivo*, providing long-lived luminescent signal in the presence of luciferase-expressing cultured cells and tissues.⁵ Of note, imaging of deeper tissues (>500 μm to cm) requires the use of near-infrared (NIR) light because hemoglobin and water exhibit their lowest absorption coefficient in the NIR window around 650–900 nm,⁶ indicating FLuc/D-luciferin exhibits

¹Department of Microbiology and Immunology, Faculty of Medicine, Hokkaido University, Sapporo, Hokkaido 060-8638, Japan

²Institute for Vaccine Research and Development (IVReD), Hokkaido University, Sapporo, Hokkaido 001-0021, Japan

³One Health Research Center, Hokkaido University, Sapporo, Hokkaido 060-0818, Japan

⁴Laboratory of Virus Control, Research Institute for Microbial Diseases, Osaka University, Suita, Osaka 565-0871, Japan

⁵Department of Cancer Pathology, Faculty of Medicine, Hokkaido University, Sapporo, Hokkaido 060-8638, Japan

⁶Institute for Chemical Reaction Design and Discovery (WPI-ICReDD), Hokkaido University, Sapporo, Hokkaido 001-0021, Japan

⁷Department of Hematology and Oncology, Graduate School of Medicine, Kyoto University, Kyoto, Kyoto 606-8501, Japan

⁸Division of Systems Virology, Department of Microbiology and Immunology, The Institute of Medical Science, The University of Tokyo, Tokyo, Tokyo 108-8639, Japan

⁹Graduate School of Medicine, The University of Tokyo, Tokyo, Tokyo 113-0033, Japan

¹⁰Graduate School of Frontier Sciences, The University of Tokyo, Kashiwa, Chiba 277-0882, Japan

¹¹CREST, Japan Science and Technology Agency, Kawaguchi, Saitama 332-0012, Japan

¹²International Research Center for Infectious Diseases, The Institute of Medical Science, The University of Tokyo, Tokyo, Tokyo 108-8639, Japan

¹³International Vaccine Design Center, The Institute of Medical Science, The University of Tokyo, Tokyo, Tokyo 108-8639, Japan

¹⁴Collaboration Unit for Infection, Joint Research Center for Human Retrovirus Infection, Kumamoto University, Kumamoto, Kumamoto 860-0811, Japan

¹⁵Institute for Genetic Medicine, Hokkaido University, Sapporo, Hokkaido 060-0815, Japan

¹⁶Laboratory of Virus Control, Center for Infectious Disease Education and Research, Osaka University, Suita, Osaka 565-0871, Japan

¹⁷Institute for Tenure Track Promotion, University of Miyazaki, Miyazaki, Miyazaki 889-2192, Japan

¹⁸AMED-CREST, Japan Agency for Medical Research and Development (AMED), Tokyo, Tokyo 100-0004, Japan

¹⁹These authors contributed equally

²⁰Present address: Institut Pasteur, Insect-Virus Interactions Unit, Department of Virology, UMR2000, CNRS, 75015 Paris, France

²¹Lead contact

*Correspondence: s.iwano0326@gmail.com (S.I.), tanaka@med.hokudai.ac.jp (S.T.), fukut@pop.med.hokudai.ac.jp (T.F.)

<https://doi.org/10.1016/j.isci.2024.109647>



impairment of sensitivity in the deep organs including lungs and for large animals. In addition, because D-luciferin is poor biodistribution, *in vivo* BLI particularly in the brain has been hampered due to low passage of D-luciferin through the blood-brain barrier (BBB).

In virology, BLI is harnessed for investigating pathogenesis, immune responses to infection, and the efficacy of therapies *in vivo*. Indeed, several studies have used recombinant viruses containing bioluminescent reporter genes to determine viral kinetics (reviewed in the study by Hutchens et al.⁷). However, for positive-sense RNA viruses, creating such reporter strains is, mostly, challenging due to the limited loci within the viral genome that can accommodate these insertions, because the gene size of RNA viruses is typically small. Thus, the highly catalytic blue-emitting luciferase NanoLuc is a primary choice for investigating the generation of the recombinant viruses. Compared to FLuc, NanoLuc offers a 150-fold increase in luminescence, is smaller (19 kDa), and has enhanced stability.⁸ Although NanoLuc and its substrate furimazine have been reported to act well as visualization of viral dynamics,^{9,10} the short emission wavelength of NanoLuc/furimazine makes it difficult when studying infection *in vivo*, viral replication in the deep organs, such as the brains and lungs, is difficult to visualize. Also, furimazine is poorly soluble in aqueous solutions and the second-generated substrate, fluorofurimazine (FFz)¹¹ is still not yet optimized for BLI in the brain. Recently, Akaluciferase (Akaluc) and its substrate AkaLumine were developed from FLuc and D-luciferin, respectively, to overcome this. The all-engineered BLI system composed of AkaLumine-HCl and Akaluc named AkaBLI emits 650 nm light, resulting in the production of more than 10 times more detectable light per reporter molecule from lungs.¹² Moreover, the AkaLumine exhibits enhanced biodistribution in most tissues including brain, indicating the AkaBLI enables to visualize the red-shifted light in whole body. Indeed, other groups have successfully visualized the cells expressing Akaluc in live animals.^{13,14}

Here, in this study, we chose severe acute respiratory syndrome coronavirus-2 (SARS-CoV-2) for investigating not only whether Akaluc can be accommodated into viral genome but whether the recombinant viruses carrying the Akaluc can be applicable *in vivo* utility. SARS-CoV-2 is a single-stranded, positive-sense RNA virus of the *Coronaviridae* family and the causative agent of COVID-19, mostly characterized as a respiratory disease.¹⁵ As SARS-CoV-2 has circulated in human populations, new variants have repeatedly emerged,¹⁶ sparking continued research. In the previous study, we found evidence that a SARS-CoV-2 variant of the Omicron lineage had evolved to have altered usage of the serine protease TMPRSS2,¹⁷ exhibiting a different pattern of replication. We generated a recombinant SARS-CoV-2 of the early pandemic lineages B.1.1 encoding codon-optimized Akaluc and showed that the recombinant virus carrying the codon-optimized Akaluc replicates comparable to the parental virus in cell culture. Then, we generated the chimeric recombinant SARS-CoV-2 carrying the spike (S) protein of the B.1.351.1 (Beta); the Omicron subvariant BA.1; or the recent Omicron subvariant XBB.1.5. Then, we investigated whether AkaBLI would reflect the differences in tissue tropism that have been observed for selected variants. In addition, we used AkaBLI to evaluate the protection conferred by licensed neutralizing monoclonal antibodies¹⁸ and mRNA vaccine¹⁹ for COVID-19.

RESULTS

Characterization of SARS-CoV-2 carrying the Akaluc luciferase gene *in vitro*

First, we produced cDNA clones of SARS-CoV-2 B.1.1 containing the wild-type Akaluc gene in place of viral open reading frames (ORFs) 6–8, which encode accessory proteins (Figure 1A).²⁰ However, infectious virus could not be recovered from transfected cells (Figure 1B). As the GC content of SARS-CoV-2 is relatively low (ca. 38%), we generated a mutant Akaluc carrying synonymous substitutions to optimize the GC content (Figure S1). As shown in Figure 1B, cytopathic effects were observed in the cells transfected with SARS-CoV-2 containing this optimized Akaluc, suggesting that the genetic fitness of foreign genes is critical for viral propagation.

The resultant virus termed B.1.1-Akaluc was subjected to northern blot analyses to confirm viral RNA synthesis. As expected, since ORFs 6–8 were replaced with the codon-optimized Akaluc, only five, instead of eight, subgenomic RNAs were detected in cells infected with B.1.1-Akaluc. The four subgenomic RNAs from ORF1a/1b and S were larger than those in the parental strain, one RNA from Akaluc gene and the other RNAs were similar in size (Figure 1C), indicating the Akaluc gene was incorporated into the viral genome and successfully maintained in descendant viral RNA. To investigate the viral properties of the recombinant virus carrying the optimized Akaluc in cell culture, VeroE6 cells expressing human TMPRSS2 (VeroE6/TMPRSS2 cells²¹) were infected with either B.1.1 or B.1.1-Akaluc at a multiplicity of infection (MOI) of 0.001, and the replication kinetics of the viruses were evaluated. The infectious titers of culture supernatants (Figure 1D, left panel) and intracellular viral RNA levels (Figure 1D, middle panel) were comparable over time for the two viruses. As expected, luciferase activity (Figure 1D, right panel) was only detected in cultures infected with B.1.1-Akaluc, mirroring the kinetics observed for intracellular viral RNA. These results indicated that replacing ORFs 6–8 of the B.1.1 genome with the Akaluc gene did not affect viral replication or production of infectious particles *in vitro*.

Next, to examine the stability of the reporter gene in B.1.1-Akaluc, we serially passaged the virus in HEK293-3P6C33 cells (express ACE2 and TMPRSS2)²² for five rounds. As shown by PCR amplification using virus-specific primers and by sequencing (Table 1, Figure S2A), the Akaluc gene was steadily maintained, suggesting that the codon-optimized Akaluc gene was stable in the B.1.1 genome. We thereafter employed the codon-optimized Akaluc for further investigations. Of note, the recombinant B.1.1, B.1.351.1, BA.1, and XBB.1.5 carrying the codon-optimized Akaluc was named “B.1.1-Akaluc, B.1.351.1-Akaluc, BA.1-Akaluc, and XBB.1.5-Akaluc”, respectively.

Evaluation of *in vivo* viral dynamics of SARS-CoV-2 by AkaBLI

Syrian hamsters support SARS-CoV-2 infection and are thus used as a small animal model for *in vivo* study.²³ First, to confirm the pathogenicity of the Akaluc recombinant virus *in vivo*, we inoculated hamsters intranasally with either B.1.1 or B.1.1-Akaluc (n = 6 per group). Weight was monitored daily for 7 days post-infection (dpi) (Figure 2A). Consistent with our previous studies,^{24–33} uninfected hamsters gained weight daily. In contrast, the infected hamsters exhibited weight loss, with the decline in weight greater in hamsters infected with B.1.1 vs. those infected with B.1.1-Akaluc. A substantial amount of viral RNA was detected in oral swabs from the day after the infection, but the copy number was

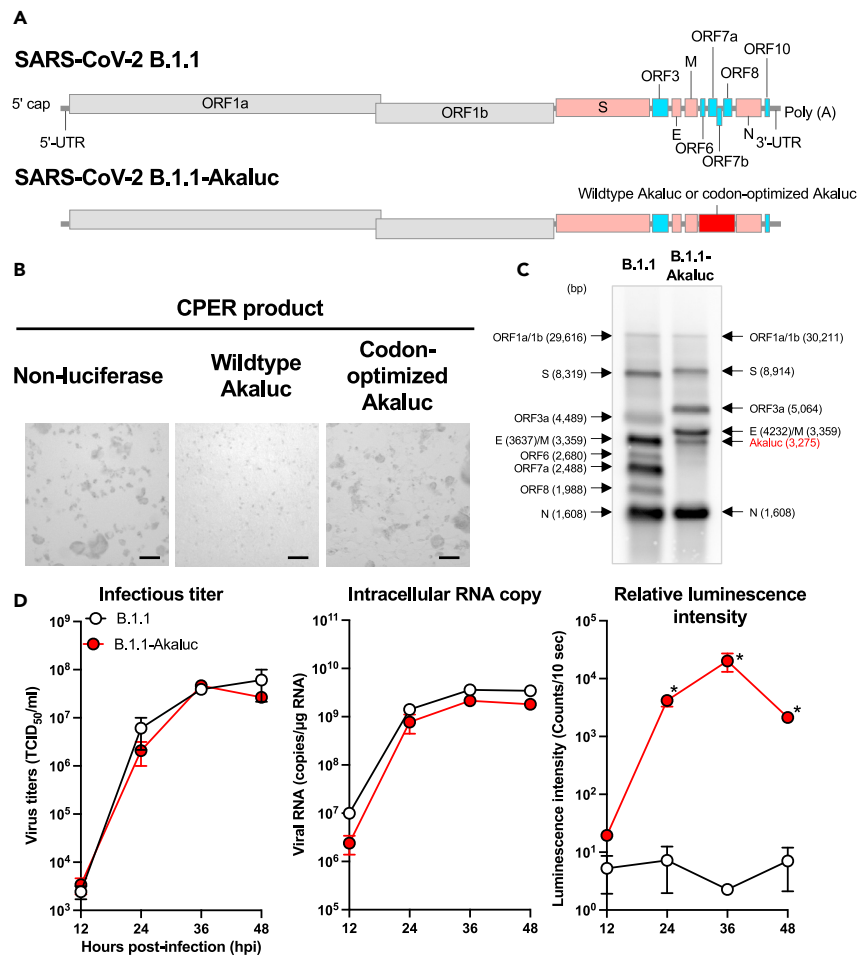


Figure 1. The virological features of SARS-CoV-2 Akaluc in vitro

(A) The gene structures of wild-type SARS-CoV-2 (B.1.1) and SARS-CoV-2 carrying either the wild type or codon-optimized Akaluc luciferase gene in place of ORFs 6–8.

(B) Viral production was judged by observation of cytopathic effects upon transfection with the transfection of each CPER product for 3 respective genomes. Representative images are shown from 6 days post transfection. Scale bars: 100 μ m.

(C) Northern blot analysis of subgenomic RNAs (sgRNAs). RNA was extracted from VeroE6/TMPRSS2 cells infected with B.1.1 or B.1.1-Akaluc and subjected to northern blot analysis. Black arrows indicate the bands for each sgRNA with size in parentheses.

(D) Growth kinetics of B.1.1 and B.1.1-Akaluc *in vitro*. VeroE6/TMPRSS2 cells were infected with either B.1.1 or B.1.1-Akaluc (MOI = 0.001). Infectious titers in the culture supernatants (left panel), the copy number of intracellular viral RNA (middle panel), and the luciferase activity (right panel) were determined at the indicated timepoints. The luminescence intensity was normalized with the signals acquired from uninfected VeroE6/TMPRSS2 cells. Asterisks indicate significant differences (*, $p < 0.05$) with the results of the wild-type virus. The presented data are expressed as the average \pm SEM. Assays were performed independently in duplicate.

higher with B.1.1 infection compared to B.1.1-Akaluc (Figure S2B). These observations suggest that the B.1.1-Akaluc was still able to replicate in hamsters but with slightly attenuated pathogenicity, leading to impairment of viral kinetics *in vivo*, likely due to insertion of the foreign gene and lack of some accessory proteins.

Next, to investigate the utility of B.1.1-Akaluc for *in vivo* imaging, we assessed Akaluc signals every 24 h up to 7 dpi and again at 10 dpi by IVIS Spectrum imaging (Figures 2B and 2C). At 1 dpi, signal was detected in the nasal cavity and then in the lungs from days 3–7 post-infection

Table 1. Mutations of the B.1.1-Akaluc after the serial passages

Position ^a	Reference	ALT	Gene	Amino acid change
17988	G	A	NSP13	No

^aRefer the nucleotide sequence of SARS-CoV-2 Wuhan-Hu-1 (GenBank: NC_045512.2).

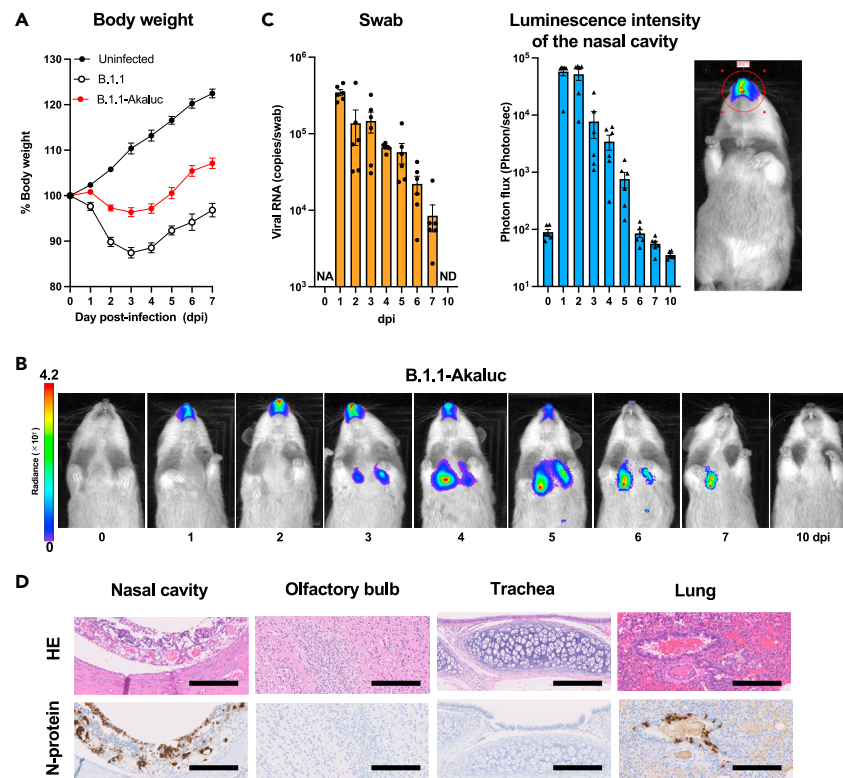


Figure 2. The virological features of B.1.1-Akaluc *in vivo*

(A) Syrian hamsters ($n = 6$ per group) were intranasally inoculated with saline, B.1.1, or B.1.1-Akaluc. Body weight was measured daily through 7 days post-infection (dpi).

(B) *In vivo* bioluminescence imaging of hamsters inoculated with B.1.1-Akaluc was performed daily through 7 dpi and again at 10 dpi. A representative image from an infected hamster is shown. The image was acquired after intraperitoneal injection of AkaLumine-HCl (75 nmol/g).

(C) Syrian hamsters ($n = 6$) were intranasally inoculated with B.1.1-Akaluc. Viral RNA copies in the oral swab (left panel) and the luminescence intensity of the nasal cavity of hamsters inoculated with B.1.1-Akaluc were measured every 24 h through 7 dpi and then again at 10 dpi. NA: Not applicable. ND: Not detected. The area of measurement of the luminescence intensity are shown in the representative image (right panel).

(D) IHC of the viral N protein (stained brown) in the nasal cavity, olfactory bulb, trachea, and lungs of hamsters at 3 dpi with B.1.1-Akaluc. Representative figures are shown. Scale bars: 200 μm . HE, hematoxylin and eosin.

(A and C) The presented data are expressed as the average \pm SEM.

(Figure 2B), indicating that B.1.1-Akaluc was able to spread through the trachea and reach the lungs after intranasal injection. Starting at 6 dpi, signal was no longer observed in the nasal cavity and by 10 dpi, not in the lungs either. Importantly, the viral RNA copies in oral swabs corresponded with the strength of the Akaluc signals measured in the nasal cavity ($R^2 = 0.5459$, $Y = 1.4325X - 3.533$; Figure S2C).

To further investigate the relationship between the Akaluc signals and viral replication in hamsters, viral nucleocapsid (N) protein was assessed by immunohistochemical (IHC) analysis in formalin-fixed organs, including the nasal cavity, olfactory bulb, trachea, and lungs, at 3 dpi. In the hamsters infected with B.1.1-Akaluc, N-positive cells were observed in the nasal cavity and the alveolar space around the bronchi/bronchioles of the lungs (Figure 2D). In contrast, N-positive cells were rarely detected in the olfactory bulb and epithelial cells of the trachea. These histological findings reflected the location of the signals visualized by AkaBLI.

NanoLuc has been used for *in vivo* imaging in studies of SARS-CoV-2 in transgenic mice expressing human ACE2 (hACE2)^{34,35} and humanized mice engrafted with human fetal lung xenografts in the skin.⁹ To assess whether NanoLuc signals can be used in hamsters, we generated recombinant B.1.1 carrying the NanoLuc gene (B.1.1-NanoLuc) in the same cassette as previously reported.³⁶ Although B.1.1-NanoLuc replicated efficiently, with strong, specific signals observed in cell culture using IVIS Spectrum imaging (Figure S2D), no NanoLuc signals were detected in hamsters when using the FFz substrate which is developed for *in vivo* usage¹¹ (Figure 3A) despite viral RNA being serially detected in oral swabs (Figure 3B). When we euthanized the inoculated animals and then directly administered FFz into the pleural cavity, the NanoLuc signals were able to be visualized (Figure S2E). Viral RNA copies in the lungs of the B.1.1-NanoLuc-infected hamsters were comparable to those in the B.1.1-Akaluc-infected hamsters at 3 dpi. Overall, these data indicate that Akaluc, but not NanoLuc, allows for visualization of the *in vivo* dynamics of SARS-CoV-2 infection in the respiratory system, including the lungs, of hamsters.

As shown in numerous studies, SARS-CoV-2 evolves as it circulates among humans.¹⁵ The Omicron variants have altered usage of TMPRSS2, the receptor for viral entry, and consequently replicate more in the upper respiratory system compared to ancestral

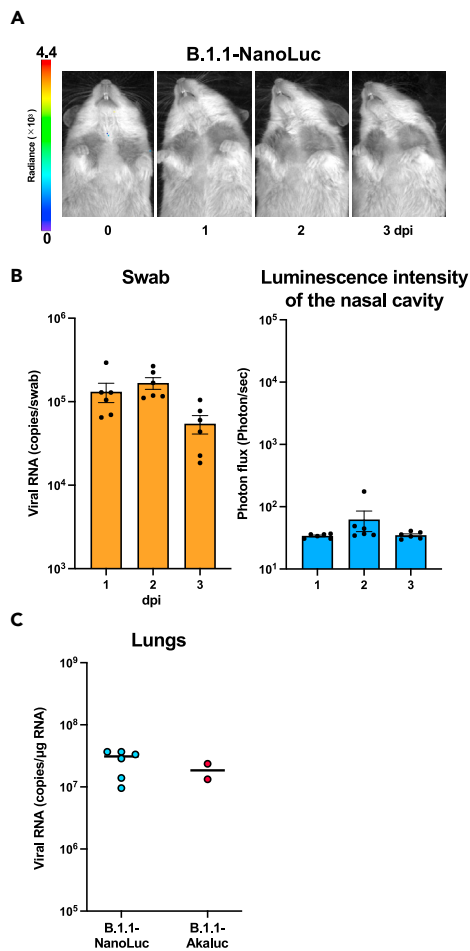


Figure 3. The virological features of B.1.1-NanoLuc in vivo

(A and B) Syrian hamsters ($n = 6$) were inoculated with B.1.1 carrying the NanoLuc luciferase gene (B.1.1-NanoLuc). Bioluminescence imaging of hamsters was performed daily through 3 dpi and a representative image from an infected hamster is shown (A). Oral swabs were collected (B, left panel) and the luminescence intensity of the nasal cavity (B, right panel) measured daily through 3 dpi. The images were acquired after intraperitoneal injection of FFz (440 nmol/g). (C) The lung hilum was harvested at 3 dpi and for quantification of viral RNA. Two hamsters infected with B.1.1-Akaluc served as controls. (B and C) The presented data are expressed as the average \pm SEM.

SARS-CoV-2.¹⁷ To investigate whether AkaBLI can assess the differences in infection of SARS-CoV-2 variants, we generated two additional recombinant viruses carrying the S gene from the ancestral lineage B.1.351.1 and the Omicron lineage BA.1, (B.1.351.1-Akaluc and BA.1-Akaluc, respectively). As observed for B.1.1-Akaluc, B.1.351.1-Akaluc, and BA.1-Akaluc replicated and exhibited Akaluc signals in cell culture infections (Figure S2F). As shown in Figure 4A, the two Omicron variants carrying the codon-optimized Akaluc replicated in hamsters, with Akaluc signal detectable starting at 1 dpi. B.1.351.1-Akaluc displayed similar distribution of Akaluc signal as B.1.1-Akaluc, with signals detected in the lungs at 3 dpi. In contrast, BA.1-Akaluc signals remained limited to the nasal cavity at 3 dpi. The strength of Akaluc signals corresponded to viral RNA copies in the oral swabs (Figure 4B). Consistent with the BLI observations, the viral RNA copies in the lungs of BA.1-Akaluc-infected hamsters were significantly lower than those of the B.1.351.1-Akaluc-infected hamsters (Figure 4C). N-positive cells as detected by IHC also corresponded with the Akaluc signals observed in the different tissues analyzed (Figures 4D and S3). Consistent with the Akaluc signal, N-positive cells were observed in bronchial epithelium in addition to nasal cavity in B.1.351.1-Akaluc-infected hamsters, whereas few N-positive cells were observed in the lung section of BA.1-Akaluc-infected hamsters (Figures 4D and 4E). These data indicate that the Akaluc signals can reflect the replication properties of SARS-CoV-2 variants.

Evaluation of *in vivo* efficacy against licensed SARS-CoV-2 antiviral and vaccine by AkaBLI

Several studies, including ours, showed that the Omicron subvariant XBB.1.5 has evolved to escape humoral immunity against the ancestral SARS-CoV-2 infection and/or vaccination.^{33,37,38} Thus, to examine whether AkaBLI can evaluate the immunoprophylactic capacity of antiviral or vaccine against SARS-CoV-2 variants, we generated recombinant, the codon-optimized Akaluc-carrying SARS-CoV-2 encoding the XBB.1.5 S protein (XBB.1.5-Akaluc). We administered neutralizing monoclonal antibodies (AZD7442)¹⁸ currently used in humans to hamsters

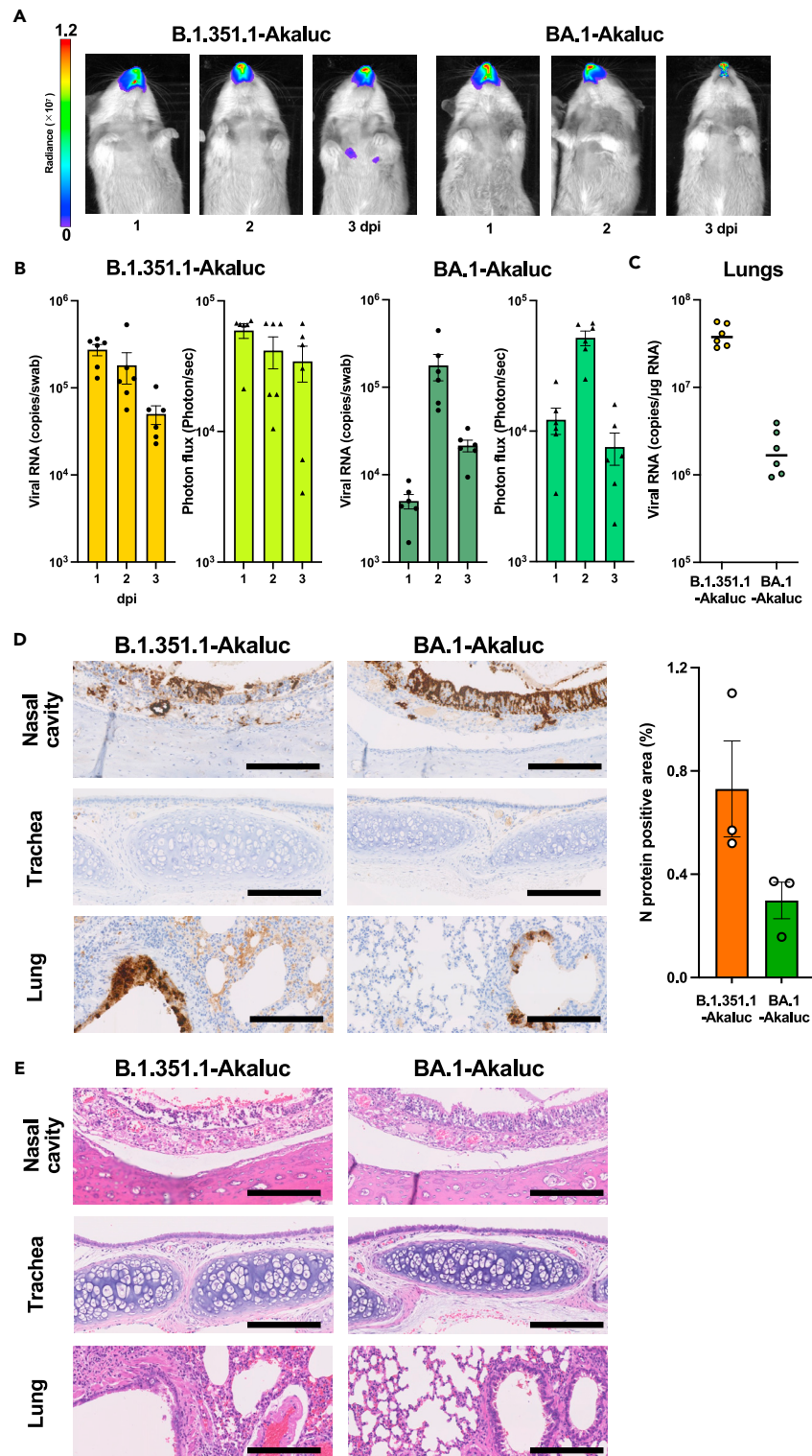


Figure 4. The virological features of SARS-CoV-2-Akaluc variants *in vivo*

Syrian hamsters ($n = 6$ per group) were intranasally inoculated with B.1.351.1-Akaluc and BA.1-Akaluc.

(A) Akaluc bioluminescence imaging of hamsters inoculated with the two viruses was performed daily through 3 dpi. Representative images are shown. The images were acquired after intraperitoneal injection of AkaLumine-HCl (75 nmol/g).

(B) Viral RNA was quantified in oral swabs and the luminescence intensity of the nasal cavity of hamsters was measured daily through 3 dpi.

Figure 4. Continued

(C) At 3 dpi, the lung hilum was harvested from hamsters and the viral RNA levels quantified.

(D) IHC of the viral N protein (stained in brown) was assessed in the nasal cavity, trachea, and lungs at 3 dpi. Representative figures are shown. Scale bars: 100 μm . Percentage of N-positive cells in whole lung lobes ($n = 3$ per infection group) are shown (right panel). See Figure S3 showing the sections of all four lung lobes.

(E) H&E staining of the areas in Figure 4D was shown.

(B and C) The presented data are expressed as the average \pm SEM.

one day prior to inoculation with either B.1.1-Akaluc or XBB.1.5-Akaluc ($n = 6$ per group) (Figure 5A). Unlike the hamsters who received the isotype control antibody, those who received AZD7442 prior to inoculation with B.1.1-Akaluc exhibited diminished Akaluc signals in the nasal cavity and no signals in the lungs (Figure 5B, upper panels), indicating AZD7442 provided protection from viral spread. In contrast, XBB.1.5-Akaluc infection resulted in a significant expression of BLI signals in the lung at 2 dpi from both antibody-administrated and non-administrated groups (Figure 5B, bottom panels). Viral RNA levels in the lungs were comparable between the two groups (Figure 5C).

Finally, to examine the utility of AkaBLI for evaluating the immunoprophylactic effects of mRNA vaccination, we used mouse-adapted SARS-CoV-2 (MA10)³⁹ to generate recombinant, Akaluc-carrying SARS-CoV-2 encoding BA.1 S (BA.1-MA10-Akaluc). Mice were immunized twice with the licensed mRNA vaccine mRNA-1273¹⁹ and efficiently produced neutralizing antibodies against SARS-CoV-2 (Figure S2G). Five weeks after the second vaccination, control and immunized mice were challenged with BA.1-MA10-Akaluc (Figure 5D). At 3 days post-challenge, Akaluc signal (Figure 5E) and viral RNA (Figure 5F) were detected in the lungs of control, but not immunized, mice. Taken together, these data indicate that AkaBLI can evaluate the effects of immunoprophylaxis and immunotherapy against SARS-CoV-2 variants.

DISCUSSION

BLI is a powerful tool for investigating *in vivo* dynamics in virology. Several studies have been attempted to generate replication-competent recombinant RNA viruses incorporating with the bioluminescent reporter for BLI.⁴⁰ However, BLI for fully visualizing viral dynamics is still challenging. This is because recombinant viruses carrying a reporter failed to propagate due to difficulties of maintaining transgene within viral genome and a lack of luciferase/luciferin for visualizing whole tissue sufficiently. Thus, limited numbers of application have been available currently in virus research. In the present study, we aimed to expand the availability of BLI for RNA viruses using the improved BLI system AkaBLI.

In previous studies, including ours, reporter genes have been accommodated into the loci of SARS-CoV-2 that encode accessory viral proteins.^{20,35,36} Thus, we attempted to replace viral ORFs 6–8 with the Akaluc gene but were unable to recover Akaluc-carrying viruses after transfecting cells with this modified genome (Figure 1B). Since the GC content of SARS-CoV-2 RNA is as low as 38% and that of the Akaluc gene is greater, we hypothesized that the GC ratio could affect the stability of foreign genes in the viral genome. We engineered a mutant Akaluc carrying synonymous substitutions to lower the gene's GC content, resulting in 42% of the GC content of the codon-optimized Akaluc from 58% of the wild-type Akaluc (Figure S1). The recombinant SARS-CoV-2 carrying this modified Akaluc exhibited robust replication in cell culture with infection kinetics similar to the parental B.1.1 genome (Figure 1D). These data suggest that the GC content of foreign genes should match that of the viral genome since GC content plays a critical role in viral propagation. Further investigations are needed to reveal the complete picture of the effect of GC content on the viral life cycle.

Several groups have reported that visualization of the *in vivo* dynamics of SARS-CoV-2 is possible with NanoLuc BLI in hACE2 transgenic mice^{34,35} expressing the primary receptor of SARS-CoV-2⁴¹ and mice engrafted with human fetal lung xenografts in the skin.⁹ However, in the present study, NanoLuc signals could only be detected by IVIS in cell culture (Figure S2D) and not in hamsters infected with recombinant SARS-CoV-2 carrying NanoLuc (Figure 3A). This is because (i) sensitivity of NanoLuc/FFz is lower than that of AkaBLI in the lungs⁴²; (ii) the hACE2 transgenic mice enables robust viral replication not only in the respiratory tissues but also in nontarget organs where the signals are easy to transpire. On the other hand, AkaBLI enabled spatiotemporal observation of recombinant SARS-CoV-2 infection dynamics in hamsters without exogenous overexpression of hACE2 (Figure 2B). To overcome transability of NanoLuc/FFz, bioluminescence resonance energy transfer (BRET)⁴³ technology might help enhanced sensitivity of viral dynamics in the lungs if the sufficient fluorescent signals were produced and should be investigated in future studies. Overall, AkaBLI is ideal for *in vivo* imaging of SARS-CoV-2 infection up to date.

The insertion of the Akaluc gene did impair SARS-CoV-2 infection in hamsters and resulted in attenuation of viral kinetics *in vivo* (Figures 2A and S2B). In this study, we replaced ORFs 6–8 with the Akaluc gene. These accessory genes are dispensable for viral replication but are reported to be involved in immune response and pathogenicity.⁴⁴ Accordingly, the lack of these genes in our B.1.1-Akaluc may have resulted in the attenuated pathogenicity we observed in hamsters, suggesting that we need to prepare pair of Akaluc-carrying recombinants that share the same backbone when we employ AkaBLI to investigate comparative pathogenicity as shown in Figure 3. Notably, in the respiratory organs of the hamsters, Akaluc signals were correlated with the levels of viral RNA in the oral swabs and reflected viral dynamics (Figures 2B, 2C, and S2C).

Numerous studies, including ours, have shown that the tissue tropism and replication properties of SARS-CoV-2 have changed during circulation among humans.^{17,24–33} In Figures 4 and 5, the recombinant viruses carrying the S of the variants B.1.351.1, BA.1, and XBB.1.5 displayed different replication dynamics in hamsters and this was reflected by AkaBLI. Staining of viral N protein by IHC was correlated with the strength of the Akaluc signals we observed (Figures 2D, 4D, and S3). Regarding the mouse-adapted SARS-CoV-2 MA10,³⁹ the virus acquired pulmonary tropism compared to its parental strain during adaptation into mice, leading to efficient replication in the lungs.⁴⁵ As shown in Figure 5E, Akaluc signals were detected not in nasal cavity but in the lungs of the MA10-infected mouse. Collectively, these data indicate that the AkaBLI can also be utilized to assess viral tissue tropism *in vivo*.

Most humans have experienced COVID-19 by infection and/or been vaccinated, and SARS-CoV-2 variants are continuously emerging (reviewed in the study by Carabelli et al.⁴⁶). Thus, our ability to protect against new variants is crucial for controlling the spread of infection. To

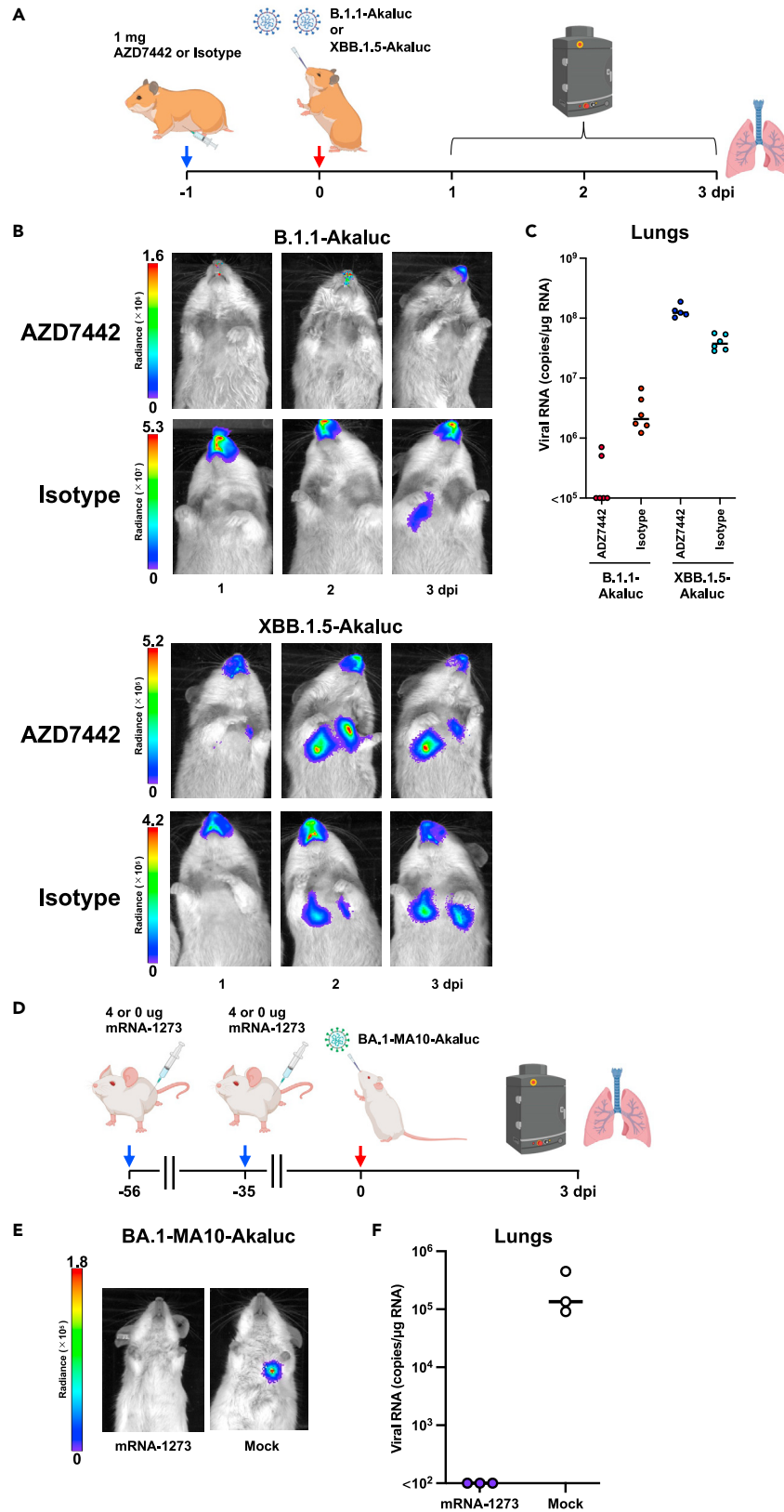


Figure 5. Evaluation of the immunoprophylactic ability of SARS-CoV-2 monoclonal antibodies and mRNA vaccine

(A) Schematic diagram of the experimental timeline for the evaluation of AZD7442 (Tixagevimab-Cilgavimab). One day before challenge, hamsters were immunized by AZD7442 (1 mg per dose) or isotype as control. Hamsters were inoculated with B.1.1-Akaluc (n = 6), or XBB.1.5-Akaluc (n = 6). One hamster in the XBB.1.5-Akaluc cohort unexpectedly died during the experiment.

(B) Akaluc bioluminescence imaging was performed daily through 3 dpi. The images were acquired after intraperitoneal injection of AkaLumine-HCl (75 nmol/g).

(C) The lung hilum was harvested at 3 dpi and subjected to viral RNA quantification. Four samples obtained from the B.1.1-Akaluc-infected hamsters administrated with AZD7442 were under detection limit of qPCR analysis.

(D) Schematic diagram of experimental timeline for the evaluation of the mRNA vaccine mRNA-1273. BALB/c mice (n = 3) were vaccinated (4 µg per dose) twice at the indicated timepoints, and the other BALB/c mice (n = 3) were not vaccinated (were received PBS as a control). Fifty-six weeks after the first vaccination, mice were inoculated with MA10-Akaluc (carrying the S protein of BA.1). Neutralizing antibody titers are shown in Figure S2F. Bioluminescence imaging was performed at 3 dpi.

(E) Representative images from infected mice (immunized and non-immunized) at 3 dpi. are shown. The images were acquired after intraperitoneal injection of AkaLumine-HCl (75 nmol/g).

(F) The lung hilum was collected at 3 dpi and subjected to viral RNA quantification.

assess whether AkaBLI can be used to evaluate antivirals, we assessed the effects of the neutralizing monoclonal antibodies AZD7442 or an mRNA vaccine on infection. Consistent with a previous report,⁴⁷ AZD7442 protected against B.1.1 but not XBB.1.5 *in vivo* (Figures 5B and 5C). In addition, to evaluate immunoprophylaxis in mice, we generated a recombinant Akaluc-carrying, mouse-adapted SARS-CoV-2.³⁹ AkaBLI was able to visualize infection with this virus in mice. As shown in Figures 5D and 5E, the mRNA vaccine fully protected mice against mouse-adapted SARS-CoV-2 infection. These findings suggest that AkaBLI can be used to investigate the *in vivo* efficacy of antivirals.

In summary, we constructed recombinant SARS-CoV-2 carrying the codon-optimized Akaluc gene and found that using AkaBLI we could monitor viral dynamics *in vivo*, evaluate differences in tissue tropism, and assess the efficacy of antivirals. Our findings, the AkaBLI together with codon-optimized luciferase, will contribute to further developments in the engineering of recombinant viruses, including those of other RNA as well as DNA viruses with wide range of tropism such as neurotropism that can be used for *in vivo* studies. The development of novel biological assays such as AkaBLI is necessary to improve our understanding of the molecular mechanisms underlying virus replication and pathogenesis as well as to preclinically evaluate new antiviral agents.

Limitations of the study

In this study, we replaced from the accessory protein genes, ORF 6–10 to the codon-optimized Akaluc and generated the recombinant viruses sufficiently useful to BLI. Although the recombinant virus carrying the codon-optimized Akaluc mirrored the *in vitro* replication to the wild-type virus (Figure 1D), the recombinant Akaluc virus exhibited the attenuated profile *in vivo* (Figures 2A and S2B). Therefore, when we discuss the viral pathogenicity using this AkaBLI, we should use the sets of recombinant viruses carrying the codon-optimized Akaluc for evaluation. Further investigations are needed for accommodation of the codon-optimized Akaluc without attenuation *in vivo*. As shown in Figure 2C, although viral RNA loads and luminescence intensity was correlated, sensitivity differed between these two. This is because detection of RNA is generally higher than detection of proteins upon viral infection. Of note, viral RNA loads do not mirror yields of viable virus particles. Together, other studies developing enhanced sensitivity of protein detection using a new pair of luciferin/luciferase and/or imaging equipment are desirable.

STAR★METHODS

Detailed methods are provided in the online version of this paper and include the following:

- KEY RESOURCES TABLE
- RESOURCE AVAILABILITY
 - Lead contact
 - Materials availability
 - Data and code availability
- EXPERIMENTAL MODEL AND STUDY PARTICIPANT DETAILS
 - Ethics statement
 - Cell culture
 - Animal experiments
 - Bioluminescence experiment
- METHOD DETAILS
 - Plasmids construction
 - SARS-CoV-2 preparation and titration
 - Northern blotting
 - Quantitative RT-PCR
 - IHC
- QUANTIFICATION AND STATISTICAL ANALYSIS

SUPPLEMENTAL INFORMATION

Supplemental information can be found online at <https://doi.org/10.1016/j.isci.2024.109647>.

ACKNOWLEDGMENTS

We thank H. Kubo, M. Tetsuka, and S. Shimamura for their secretarial work and H. Maruyama, M. Hanazaki, T. Matsuoka, M. Hommura, A. Imajoh, K. Oyama, H. Murota, and S.D. Ishikawa for their technical assistance. This work was supported in part by AMED SCARDA Hokkaido University Institute for Vaccine Research and Development (HU-IVReD) (JP23fa627005h0001 to Takasuke Fukuhara); AMED SCARDA (JP223fa827001h0001 to Takasuke Fukuhara), AMED Research Program on Emerging and Re-emerging Infectious Diseases (JP21fk0108617h0001, JP21fk0108493h0001, JP22fk0108511h0001, and JP22fk0108516h0001 to Takasuke Fukuhara); AMED Project for Advanced Drug Discovery and Development (JP21nf0101627 to Takasuke Fukuhara); AMED CREST (JP22gm1610008h0001 to Takasuke Fukuhara); JSPS KAKENHI Grant-in-Aid for Scientific Research B (21H02736 to Takasuke Fukuhara); JSPS KAKENHI Fund for the Promotion of Joint International Research (International Leading Research) (JP23K20041 to Takasuke Fukuhara); Takeda Science Foundation (to Takasuke Fukuhara); Hokuto Foundation for Bioscience (to Tomokazu Tamura); Hirose Foundation (to Tomokazu Tamura) and Hokkaido University Support Program for Frontier Research (to Takasuke Fukuhara).

AUTHOR CONTRIBUTIONS

T.T., Shiho T., and T.F. designed the research; T.T., H.I., Shiho T., L.W., R.S., Shuhei T., A.K., and Yu. M. performed the research; T.T., S.S., M.T., Kotaro S., Kei S., Yo. M., Shinya T., S.I., and T.F. analyzed the data; and T.T., H.I., S.I., and T.F. wrote the paper.

DECLARATION OF INTERESTS

The authors declare no competing interests.

Received: December 7, 2023

Revised: February 25, 2024

Accepted: March 27, 2024

Published: March 29, 2024

REFERENCES

- Green, A.A., and Mcelroy, W.D. (1956). Crystalline firefly luciferase. *Biochim. Biophys. Acta* 20, 170–176. [https://doi.org/10.1016/0006-3002\(56\)90275-x](https://doi.org/10.1016/0006-3002(56)90275-x).
- Rodriguez, J.F., Rodriguez, D., Rodriguez, J.R., McGowan, E.B., and Esteban, M. (1988). Expression of the firefly luciferase gene in vaccinia virus: a highly sensitive gene marker to follow virus dissemination in tissues of infected animals. *Proc. Natl. Acad. Sci. USA* 85, 1667–1671. <https://doi.org/10.1073/pnas.85.5.1667>.
- Sweeney, T.J., Mailänder, V., Tucker, A.A., Olomu, A.B., Zhang, W., Cao, Y.a., Negrin, R.S., and Contag, C.H. (1999). Visualizing the kinetics of tumor-cell clearance in living animals. *Proc. Natl. Acad. Sci. USA* 96, 12044–12049. <https://doi.org/10.1073/pnas.96.21.12044>.
- Kaskova, Z.M., Tsarkova, A.S., and Yampolsky, I.V. (2016). 1001 lights: luciferins, luciferases, their mechanisms of action and applications in chemical analysis, biology and medicine. *Chem. Soc. Rev.* 45, 6048–6077. <https://doi.org/10.1039/c6cs00296j>.
- Mezzanotte, L., van 't Root, M., Karatas, H., Goun, E.A., and Löwik, C.W.G.M. (2017). In Vivo Molecular Bioluminescence Imaging: New Tools and Applications. *Trends Biotechnol.* 35, 640–652. <https://doi.org/10.1016/j.tibtech.2017.03.012>.
- Weissleder, R. (2001). A clearer vision for in vivo imaging. *Nat. Biotechnol.* 19, 316–317. <https://doi.org/10.1038/86684>.
- Hutchens, M., and Luker, G.D. (2007). Applications of bioluminescence imaging to the study of infectious diseases. *Cell Microbiol.* 9, 2315–2322. <https://doi.org/10.1111/j.1462-5822.2007.00995.x>.
- Hall, M.P., Unch, J., Binkowski, B.F., Valley, M.P., Butler, B.L., Wood, M.G., Otto, P., Zimmerman, K., Vidugiris, G., Machleidt, T., et al. (2012). Engineered luciferase reporter from a deep sea shrimp utilizing a novel imidazopyrazinone substrate. *ACS Chem. Biol.* 7, 1848–1857. <https://doi.org/10.1021/cb3002478>.
- Kenney, D.J., O'Connell, A.K., Turcinovic, J., Montanaro, P., Hekman, R.M., Tamura, T., Berneshawi, A.R., Cafiero, T.R., Al Abdullatif, S., Blum, B., et al. (2022). Humanized mice reveal a macrophage-enriched gene signature defining human lung tissue protection during SARS-CoV-2 infection. *Cell Rep.* 39, 110714. <https://doi.org/10.1016/j.celrep.2022.110714>.
- Kanai, Y., Kawagishi, T., Matsuura, Y., and Kobayashi, T. (2019). Live Imaging of Oncolytic Mammalian Orthoreovirus Expressing NanoLuc Luciferase in Tumor Xenograft Mice. *J. Virol.* 93, e00401-19. <https://doi.org/10.1128/JVI.00401-19>.
- Su, Y., Walker, J.R., Park, Y., Smith, T.P., Liu, L.X., Hall, M.P., Labanieh, L., Hurst, R., Wang, D.C., Encell, L.P., et al. (2020). Novel NanoLuc substrates enable bright two-population bioluminescence imaging in animals. *Nat. Methods* 17, 852–860. <https://doi.org/10.1038/s41592-020-0889-6>.
- Iwano, S., Sugiyama, M., Hama, H., Watakabe, A., Hasegawa, N., Kuchimaru, T., Tanaka, K.Z., Takahashi, M., Ishida, Y., Hata, J., et al. (2018). Single-cell bioluminescence imaging of deep tissue in freely moving animals. *Science* 359, 935–939. <https://doi.org/10.1126/science.aag1067>.
- Ito, A., Matsuda, N., Ukita, Y., Okumura, M., and Chihara, T. (2023). Akaluc/AkaLumine bioluminescence system enables highly sensitive, non-invasive and temporal monitoring of gene expression in *Drosophila*. *Commun. Biol.* 6, 1270. <https://doi.org/10.1038/s42003-023-05628-x>.
- Bozec, D., Sattiraju, A., Bouras, A., Jesu Raj, J.G., Rivera, D., Huang, Y., Junqueira Alves, C., Tejero, R., Tsankova, N.M., Zou, H., et al. (2020). Akaluc bioluminescence offers superior sensitivity to track in vivo glioma expansion. *Neurooncol. Adv.* 2, vdaa134. <https://doi.org/10.1093/oaajnl/vdaa134>.
- WHO (2023). Coronavirus Disease 2019. <https://www.who.int/emergencies/diseases/novel-coronavirus-2019>.
- WHO (2023). Tracking SARS-CoV-2 Variants (March 15, 2023). <https://www.who.int/activities/tracking-SARS-CoV-2-variants>.
- Meng, B., Abdullahi, A., Ferreira, I.A.T.M., Goonawardane, N., Saito, A., Kimura, I., Yamasoba, D., Gerber, P.P., Fathi, S., Rathore, S., et al. (2022). Altered TMPRSS2 usage by SARS-CoV-2 Omicron impacts infectivity and fusogenicity. *Nature* 603, 706–714. <https://doi.org/10.1038/s41586-022-04474-x>.
- Dong, J., Zost, S.J., Greaney, A.J., Starr, T.N., Dings, A.S., Chen, E.C., Chen, R.E., Case, J.B., Sutton, R.E., Gilchuk, P., et al. (2021). Genetic and structural basis for SARS-CoV-2 variant neutralization by a two-antibody cocktail. *Nat. Microbiol.* 6, 1233–1244. <https://doi.org/10.1038/s41564-021-00972-2>.

19. Baden, L.R., El Sahly, H.M., Essink, B., Kotloff, K., Frey, S., Novak, R., Diemert, D., Spector, S.A., Roupheal, N., Creech, C.B., et al. (2021). Efficacy and Safety of the mRNA-1273 SARS-CoV-2 Vaccine. *N. Engl. J. Med.* 384, 403–416. <https://doi.org/10.1056/NEJMoa2035389>.
20. Torii, S., Ono, C., Suzuki, R., Morioka, Y., Anzai, I., Fauzyah, Y., Maeda, F., Kamitani, W., Fukuhara, T., and Matsuura, Y. (2021). Establishment of a reverse genetics system for SARS-CoV-2 using circular polymerase extension reaction. *Cell Rep.* 35, 109014. <https://doi.org/10.1016/j.celrep.2021.109014>.
21. Matsuyama, S., Nao, N., Shirato, K., Kawase, M., Saito, S., Takayama, I., Nagata, N., Sekizuka, T., Katoh, H., Kato, F., et al. (2020). Enhanced isolation of SARS-CoV-2 by TMPRSS2-expressing cells. *Proc. Natl. Acad. Sci. USA* 117, 7001–7003. <https://doi.org/10.1073/pnas.2002589117>.
22. Motozono, C., Toyoda, M., Zahradnik, J., Saito, A., Nasser, H., Tan, T.S., Ngare, I., Kimura, I., Uriu, K., Kosugi, Y., et al. (2021). SARS-CoV-2 spike L452R variant evades cellular immunity and increases infectivity. *Cell Host Microbe* 29, 1124–1136.e11. <https://doi.org/10.1016/j.chom.2021.06.006>.
23. Muñoz-Fontela, C., Dowling, W.E., Funnell, S.G.P., Gsell, P.S., Riveros-Balta, A.X., Albrecht, R.A., Andersen, H., Baric, R.S., Carroll, M.W., Cavaleri, M., et al. (2020). Animal models for COVID-19. *Nature* 586, 509–515. <https://doi.org/10.1038/s41586-020-2787-6>.
24. Saito, A., Irie, T., Suzuki, R., Maemura, T., Nasser, H., Uriu, K., Kosugi, Y., Shirakawa, K., Sadamasu, K., Kimura, I., et al. (2022). Enhanced fusogenicity and pathogenicity of SARS-CoV-2 Delta P681R mutation. *Nature* 602, 300–306. <https://doi.org/10.1038/s41586-021-04266-9>.
25. Saito, A., Tamura, T., Zahradnik, J., Deguchi, S., Tabata, K., Anraku, Y., Kimura, I., Ito, J., Yamasoba, D., Nasser, H., et al. (2022). Virological characteristics of the SARS-CoV-2 Omicron BA.2.75 variant. *Cell Host Microbe* 30, 1540–1555.e15. <https://doi.org/10.1016/j.chom.2022.10.003>.
26. Yamasoba, D., Kimura, I., Nasser, H., Morioka, Y., Nao, N., Ito, J., Uriu, K., Tsuda, M., Zahradnik, J., Shirakawa, K., et al. (2022). Virological characteristics of the SARS-CoV-2 Omicron BA.2 spike. *Cell* 185, 2103–2115.e19. <https://doi.org/10.1016/j.cell.2022.04.035>.
27. Suzuki, R., Yamasoba, D., Kimura, I., Wang, L., Kishimoto, M., Ito, J., Morioka, Y., Nao, N., Nasser, H., Uriu, K., et al. (2022). Attenuated fusogenicity and pathogenicity of SARS-CoV-2 Omicron variant. *Nature* 603, 700–705. <https://doi.org/10.1038/s41586-022-04462-1>.
28. Kimura, I., Yamasoba, D., Tamura, T., Nao, N., Suzuki, T., Oda, Y., Mitoma, S., Ito, J., Nasser, H., Zahradnik, J., et al. (2022). Virological characteristics of the SARS-CoV-2 Omicron BA.2 subvariants, including BA.4 and BA.5. *Cell* 185, 3992–4007.e16. <https://doi.org/10.1016/j.cell.2022.09.018>.
29. Ito, J., Suzuki, R., Uriu, K., Itakura, Y., Zahradnik, J., Kimura, K.T., Deguchi, S., Wang, L., Lytras, S., Tamura, T., et al. (2023). Convergent evolution of SARS-CoV-2 Omicron subvariants leading to the emergence of BQ.1.1 variant. *Nat. Commun.* 14, 2671. <https://doi.org/10.1038/s41467-023-38188-z>.
30. Tamura, T., Ito, J., Uriu, K., Zahradnik, J., Kida, I., Anraku, Y., Nasser, H., Shofa, M., Oda, Y., Lytras, S., et al. (2023). Virological characteristics of the SARS-CoV-2 XBB variant derived from recombination of two Omicron subvariants. *Nat. Commun.* 14, 2800. <https://doi.org/10.1038/s41467-023-38435-3>.
31. Tamura, T., Yamasoba, D., Oda, Y., Ito, J., Kamasaki, T., Nao, N., Hashimoto, R., Fujioka, Y., Suzuki, R., Wang, L., et al. (2023). Comparative pathogenicity of SARS-CoV-2 Omicron subvariants including BA.1, BA.2, and BA.5. *Commun. Biol.* 6, 772. <https://doi.org/10.1038/s42003-023-05081-w>.
32. Tamura, T., Mizuma, K., Nasser, H., Deguchi, S., Padilla-Blanco, M., Oda, Y., Uriu, K., Tolentino, J.E.M., Tsujino, S., Suzuki, R., et al. (2024). Virological characteristics of the SARS-CoV-2 BA.2.86 variant. *Cell Host Microbe* 32, 170–180.e12. <https://doi.org/10.1016/j.chom.2024.01.001>.
33. Tamura, T., Irie, T., Deguchi, S., Yajima, H., Tsuda, M., Nasser, H., Mizuma, K., Plianchaisuk, A., Suzuki, S., Uriu, K., et al. (2024). Virological characteristics of the SARS-CoV-2 Omicron XBB.1.5 variant. *Nat. Commun.* 15, 1176. <https://doi.org/10.1038/s41467-024-45274-3>.
34. Ullah, I., Prévost, J., Ladinsky, M.S., Stone, H., Lu, M., Anand, S.P., Beaudoin-Bussièrès, G., Symmes, K., Benlarbi, M., Ding, S., et al. (2021). Live imaging of SARS-CoV-2 infection in mice reveals that neutralizing antibodies require Fc function for optimal efficacy. *Immunity* 54, 2143–2158.e15. <https://doi.org/10.1016/j.immuni.2021.08.015>.
35. Ye, C., Chiem, K., Park, J.G., Silvas, J.A., Morales Vasquez, D., Sourimant, J., Lin, M.J., Greninger, A.L., Plemper, R.K., Torrelles, J.B., et al. (2021). Analysis of SARS-CoV-2 infection dynamic in vivo using reporter-expressing viruses. *Proc. Natl. Acad. Sci. USA* 118, e2111593118. <https://doi.org/10.1073/pnas.2111593118>.
36. Xie, X., Muruato, A.E., Zhang, X., Lokugamage, K.G., Fontes-Garfias, C.R., Zou, J., Liu, J., Ren, P., Balakrishnan, M., Cihlar, T., et al. (2020). A nanoluciferase SARS-CoV-2 for rapid neutralization testing and screening of anti-infective drugs for COVID-19. *Nat. Commun.* 11, 5214. <https://doi.org/10.1038/s41467-020-19055-7>.
37. Yue, C., Song, W., Wang, L., Jian, F., Chen, X., Gao, F., Shen, Z., Wang, Y., Wang, X., and Cao, Y. (2023). Enhanced transmissibility of XBB.1.5 is contributed by both strong ACE2 binding and antibody evasion. Preprint at bioRxiv 7. <https://doi.org/10.1101/2023.01.03.522427>.
38. Uriu, K., Ito, J., Zahradnik, J., Fujita, S., Kosugi, Y., Schreiber, G.; Genotype to Phenotype Japan G2P-Japan Consortium, and Sato, K. (2023). Enhanced transmissibility, infectivity, and immune resistance of the SARS-CoV-2 omicron XBB.1.5 variant. *Lancet Infect. Dis.* 23, 280–281. [https://doi.org/10.1016/S1473-3099\(23\)00051-8](https://doi.org/10.1016/S1473-3099(23)00051-8).
39. Leist, S.R., Dinnon, K.H., Schäfer, A., Tse, L.V., Okuda, K., Hou, Y.J., West, A., Edwards, C.E., Sanders, W., Fritch, E.J., et al. (2020). A Mouse-Adapted SARS-CoV-2 Induces Acute Lung Injury and Mortality in Standard Laboratory Mice. *Cell* 183, 1070–1085.e12. <https://doi.org/10.1016/j.cell.2020.09.050>.
40. Coleman, S.M., and McGregor, A. (2015). A bright future for bioluminescent imaging in viral research. *Future Virol.* 10, 169–183. <https://doi.org/10.2217/fvl.14.96>.
41. Oladunni, F.S., Park, J.G., Pino, P.A., Gonzalez, O., Akhter, A., Allué-Guardia, A., Olmo-Fontánez, A., Gautam, S., Garcia-Vilanova, A., Ye, C., et al. (2020). Lethality of SARS-CoV-2 infection in K18 human angiotensin-converting enzyme 2 transgenic mice. *Nat. Commun.* 11, 6122. <https://doi.org/10.1038/s41467-020-19891-7>.
42. Gaspar, N., Walker, J.R., Zambito, G., Marella-Panth, K., Lowik, C., Kirkland, T.A., and Mezzanotte, L. (2021). Evaluation of NanoLuc substrates for bioluminescence imaging of transferred cells in mice. *J. Photochem. Photobiol., B* 216, 112128. <https://doi.org/10.1016/j.jphotobiol.2021.112128>.
43. Kobayashi, H., Picard, L.P., Schönege, A.M., and Bouvier, M. (2019). Bioluminescence resonance energy transfer-based imaging of protein-protein interactions in living cells. *Nat. Protoc.* 14, 1084–1107. <https://doi.org/10.1038/s41596-019-0129-7>.
44. Redondo, N., Zaldívar-López, S., Garrido, J.J., and Montoya, M. (2021). SARS-CoV-2 Accessory Proteins in Viral Pathogenesis: Knowns and Unknowns. *Front. Immunol.* 12, 708264. <https://doi.org/10.3389/fimmu.2021.708264>.
45. Thieulent, C.J., Dittmar, W., Balasuriya, U.B.R., Crossland, N.A., Wen, X., Richt, J.A., and Carossino, M. (2023). Mouse-Adapted SARS-CoV-2 MA10 Strain Displays Differential Pulmonary Tropism and Accelerated Viral Replication, Neurodissemination, and Pulmonary Host Responses in K18-hACE2 Mice. *mSphere* 8, e0055822. <https://doi.org/10.1128/msphere.0055822>.
46. Carabelli, A.M., Peacock, T.P., Thorne, L.G., Harvey, W.T., Hughes, J., COVID-19 Genomics UK Consortium, Peacock, S.J., Barclay, W.S., de Silva, T.I., Towers, G.J., and Robertson, D.L. (2023). SARS-CoV-2 variant biology: immune escape, transmission and fitness. *Nat. Rev. Microbiol.* 21, 162–177. <https://doi.org/10.1038/s41579-022-00841-7>.
47. Bruel, T., Vrignaud, L.L., Porrot, F., Staropoli, I., Planas, D., Guivel-Benhassine, F., Puech, J., Prot, M., Munier, S., Bolland, W.H., et al. (2023). Sotrovimab therapy elicits antiviral activities against Omicron BQ.1.1 and XBB.1.5 in sera of immunocompromised patients. *Med* 4, 664–667. <https://doi.org/10.1016/j.medj.2023.07.007>.
48. Ozono, S., Zhang, Y., Tobiume, M., Kishigami, S., and Tokunaga, K. (2020). Super-rapid quantitation of the production of HIV-1 harboring a luminescent peptide tag. *J. Biol. Chem.* 295, 13023–13030. <https://doi.org/10.1074/jbc.RA120.013887>.
49. Reed, L., and Muench, H. (1938). A simple method of estimating fifty per cent endpoints. *Am. J. Hyg.* 27, 493–497.

STAR★METHODS

KEY RESOURCES TABLE

REAGENT or RESOURCE	SOURCE	IDENTIFIER
Chemicals, peptides, and recombinant proteins		
DMEM (high glucose)	Nacalai Tesque	Cat#08459-34
DMEM (low glucose)	FUJIFILM Wako Chemicals	Cat#041-29775
Fetal bovine serum	BioWest	Cat#S1810-500
Penicillin-Streptomycin Mixed Solution (Stabilized)	Nacalai Tesque	Cat#09367-34
G 418 Disulfate Aqueous Spltion	Nacalai Tesque	Cat#09380-44
TransIT-LT1	Mirus Bio	Cat#MIR2306
Doxycycline	InvivoGen	N/A
Opti-MEM	Thermo Fisher Scientific	Cat#31985-070
Medetomidine hydrochloride (Domitor)	Nippon Zenyaku Kogyo	N/A
Butorphanol tartrate (Vetorphale)	Meiji Seika Pharma	N/A
Alphaxalone (Alfaxan)	Jurox Pty Limited	N/A
DIG wash and block buffer set	Sigma-Aldrich	Cat#11585762001
CDP-Star Chemiluminescent substrate	Sigma-Aldrich	Cat#C0721-100mL
Critical commercial assays		
DIG RNA Labeling kit (SP6/T7)	Sigma-Aldrich	Cat#1175025910
PureLink RNA Mini Kit	Thermo Fisher Scientific	Cat#12183025
One Step PrimeScript III RT-PCR Kit	Takara Bio	Cat#RR600A
PrimeSTAR GXL DNA polymerase	Takara Bio	Cat# R050A
Nano-Glo <i>In Vivo</i> Substrate	Promega	Cat# CS320501
AkaLumine-HCl	FUJIFILM Wako Chemicals	Cat#018-26703
Experimental models: Cell lines		
Human: HEK293-3P6C33 cells	Torii et al. ²⁰	N/A
African green monkey (<i>Chlorocebus sabaeus</i>): VeroE6/TMPRSS2 cells	Matsuyama et al. ²¹	N/A
Experimental models: Organisms/strains		
BALB/c mice (male, 10-week-old)	CLEA Japan Inc.	https://www.clea-japan.com/dcms_media/other/BALBcA_BLD10W_2019.pdf
Slc:Syrian hamsters (male, 4-week-old)	Japan SLC Inc.	http://www.jslc.co.jp/pdf/hamster/2020/028_Slc_Syrian.pdf
Oligonucleotides		
See Table S1		
Recombinant DNA		
pCSII-CoV-2-G1	Torii et al. ²⁰	N/A
pCSII-CoV-2-G2	Torii et al. ²⁰	N/A
pCSII-CoV-2-G3	Torii et al. ²⁰	N/A
pMW118-CoV-2-G4	This study	N/A
pcDNA3.1-CoV-2-G5	This study	N/A
pcDNA3.1-CoV-2-G6	This study	N/A
pCSII-CoV-2-G7	Torii et al. ²⁰	N/A
pcDNA3.1-CoV-2-G9-10	This study	N/A

(Continued on next page)

Continued

REAGENT or RESOURCE	SOURCE	IDENTIFIER
pMW118-CoV-2-UTRlinker	Torii et al. ²⁰	N/A
pMW118-CoV-2-G9-10-NanoLuc	This study	N/A
pcDNA3.1-CoV-2-G9-10-Akaluc	This study	N/A
pcDNA3.1-CoV-2-G9-10-Codon-optimized Akaluc	This study	N/A
pCSII-CoV-2-F8-D614G	This study	N/A
pMW118-CoV-2-F8-BA.1	This study	N/A
pMW118-CoV-2-F8-B.1.351.1	This study	N/A
pMW118-CoV-2-F8-XBB.1.5	Tamura et al. ³³	N/A
pMW118-CoV-2-F3-MA10	This study	N/A
pMW118-CoV-2-F4-MA10	This study	N/A

Other

SeqStudio Genetic Analyzer	Thermo Fisher Scientific	Cat#SEQ-CP1-D
WSE-6100LuminoGraphl	Atto	Cat#WSE-6100
QuantStudio 5 Real-Time PCR System	Thermo Fisher Scientific	N/A
IVIS Imaging System	PerkinElmer	N/A
AB-2270 Luminescencer Octa	Atto	Cat#AB-2270
OpenSource Diets	Research Diet	D10001

RESOURCE AVAILABILITY**Lead contact**

Further information and requests for resources and reagents should be directed to and will be fulfilled by the Lead Contact, Takasuke Fukuhara (fukut@pop.med.hokudai.ac.jp).

Materials availability

All unique reagents generated in this study are listed in the [key resources table](#) and available from the [lead contact](#) with a completed Materials Transfer Agreement.

Data and code availability

- Data produced in this paper is available upon request to the [lead contact](#).
- This paper does not report original code.
- Any additional information required to reanalyze the data reported in this work is available from the [lead contact](#) upon request.

EXPERIMENTAL MODEL AND STUDY PARTICIPANT DETAILS**Ethics statement**

All experiments with hamsters and mice were performed in accordance with the Science Council of Japan's Guidelines for the Proper Conduct of Animal Experiments. The protocol was approved by the Institutional Animal Care and Use Committee of National University Corporation Hokkaido University (approval number 20–0123).

Cell culture

All mammalian cell lines were cultured at 37°C under the conditions of a humidified atmosphere and 5% CO₂. HEK293 (human embryonic kidney-derived 293)-3P6C33 cells (HEK293 cells stably expressing human ACE2 and TMPRSS2)²⁰ were maintained in high-glucose Dulbecco's Modified Eagle Medium (DMEM) (Nacalai Tesque) supplemented with 100 U/mL penicillin, 100 µg/mL streptomycin (PS) (Nacalai Tesque), and 10% fetal bovine serum. African green monkey kidney-derived VeroE6/TMPRSS2 cells (VeroE6 cells stably expressing human TMPRSS2)²¹ were maintained in low-glucose DMEM (FUJIFILM Wako Chemicals) supplemented with 1 mg/mL G418 (Nacalai Tesque) and 10% fetal bovine serum.

For growth kinetics, SARS-CoV-2 was inoculated into VeroE6/TMPRSS2 cells in 6-well plates at a multiplicity of infection (MOI) of 0.01, the culture supernatants were replaced with new medium at 1 hpi and incubated for 48 h. The infectious titers of the culture supernatants collected at 12, 24, 36, and 48 hpi were then determined.

To investigate the stability of the codon-optimized Akaluc gene into the SARS-CoV-2 genome, 300,000 HEK293-3P6C33 cells/well were seeded into a 6-well plate 1 day before infection. SARS-CoV-2 carrying Akaluc was used to inoculate the HEK293-3P6C33 cells at an MOI of 1.0. At 1 hpi, the culture supernatants were replaced with new medium and then incubated for 48 h. Culture supernatants collected at 48 hpi were used as an inoculum for new HEK293-3P6C33 cells and also used for viral RNA extraction and sequence analysis (See Figure S2A; Table 1).

Animal experiments

Animal experiments were performed as previously described.^{24–33} Syrian hamsters (male, 4 weeks old) were purchased from Japan SLC Inc. BALB/c mice (male, 10 weeks old) were purchased from CLEA Japan Inc. For the virus infection experiments, animals were anesthetized by intramuscular injection with a mixture of 0.15 mg/kg medetomidine hydrochloride (Domitor, Nippon Zenyaku), 2.0 mg/kg midazolam (Dormicum, Fujifilm WAKO Chemical), and 2.5 mg/kg butorphanol (Vetorphale, Meiji Seika Pharma) or 0.15 mg/kg medetomidine hydrochloride, 4.0 mg/kg alphaxalone (Alfaxan, Jurox), and 2.5 mg/kg butorphanol. Animals were intranasally inoculated under anesthesia with the recombinant viruses (10,000 TCID₅₀ in 100 μ L for hamsters or 1,000 TCID₅₀ in 50 μ L for mice) or saline (100 μ L). Oral swabs were collected at the indicated timepoints. Body weight was recorded daily through 7 dpi. Lung tissues were anatomically collected at 3 dpi. The viral RNA load in the oral swabs and respiratory tissues was determined by quantitative RT-PCR. These tissues were also used for IHC and histopathological analyses (see below). For evaluation of *in vivo* efficacy against licensed SARS-CoV-2 antiviral and vaccine, hamsters were intramuscularly injected with 1 mg per dose of AZD7442 (Tixagevimab-Cilgavimab; AstraZeneca) one day before viral infection. Mice were received twice with 4 μ g of the mRNA vaccine RNA-1273 (Moderna) 7 and 5 weeks before virus challenge.

Bioluminescence experiment

Luminescence was detected using AkaLumine-HCl (FUJIFILM Wako Chemicals), and luciferase activity *in vitro* was measured by the 10-s integral analysis using an AB-2270 Luminescencer Octa (Atto) according to the manufacturer's protocol. VeroE6/TMPRSS2 cells were seeded in a black 96-well plate (PerkinElmer) at a density of 15,000 cells per well. Serially diluted B.1.1, B.1.1-NanoLuc, or B.1.1-Akaluc were used to infect the cells. At 32 hpi, cells were washed once with PBS and imaged using an IVIS Imager (PerkinElmer) at 5 min after addition of substrate: fluorofurimazine (FFz) (3 g/mL; Promega) for NanoLuc and AkaLumine-HCl (4.3 g/mL) for Akaluc. The following conditions were used for image acquisition: open emission filter, exposure time = 3 s, binning = medium: 8, field of view = 13.2 \times 13.2 cm and f/stop = 1.

For *in vivo* experiments, infected hamsters or mice were injected with FFz (440 nmol/g) or AkaLumine-HCl (75 nmol/g) intraperitoneally according to the indicated protocol from the previous studies^{11,12} and the luminescence images were monitored by IVIS at 1, 2, and 3 dpi. The following conditions were used for image acquisition: open emission filter, exposure time = 60 s, binning = medium: 8, field of view = 13.2 \times 13.2 cm and f/stop = 1. All images were analyzed using Living Image Ver4.7.3 (PerkinElmer).

METHOD DETAILS

Plasmids construction

To generate recombinant SARS-CoV-2, 9 plasmids were used to amplify SARS-CoV-2 cDNA fragments (F1 to F9-10) by PrimeSTAR GXL DNA polymerase (Takara Bio) with the previously reported primer sets²⁰ (See Table S1 for primer information). The amplified DNA fragments were used for circular polymerase extension reaction (CPER; see below). To generate viruses carrying the NanoLuc luciferase gene, nucleotides 27,433–27,675 in the ORF7 region of pcDNA.3.1-CoV-2-G9-10 were replaced with the NanoLuc gene as previously described,³⁶ and the resulting plasmids were designated as pcDNA.3.1-CoV-2-G9-10-NanoLuc. To generate viruses carrying the wildtype Akaluc luciferase gene (1,653 nt length),¹² the nucleotide sequences of ORFs 6–8 in pcDNA.3.1-CoV-2-G9-10 were replaced with the wildtype Akaluc gene, and the resulting plasmids were designated as pcDNA.3.1-CoV-2-G9-10-Akaluc. Codon-optimized Akaluc was synthesized and purchased (Eurofins Scientific). Then, the luciferase gene was inserted as described above. SARS-CoV-2 B.1.1 Spike carrying a D614G mutation⁴⁸ or Spike with B.1.351.1, BA.1,²⁷ or XBB.1.5³³ sequence were inserted into a pCSII or pMW vectors, and were designated as pCSII-CoV-2-G8-D614G, pMW-CoV-2-G8-B.1.351.1, pMW-CoV-2-G8-BA.1, pMW118-CoV-2-G8-XBB.1.5. To generate mouse-adapted SARS-CoV-2 (MA10), which has seven mutations (C9438U, A11847G, A12159G, C23039A, U27221C, Q498Y, P499T) to facilitate replication in mice,³⁹ these mutations were incorporated into F3 and F4 and inserted into a pMW118 vector (pMW118-SARS-CoV-2-G3-MA10, -G4-MA10). Sequences of all the plasmids used in this study were confirmed by sequencing with SeqStudio Genetic Analyzer (Thermo Fisher Scientific) and outsourced service (Fasmac).

SARS-CoV-2 preparation and titration

Recombinant SARS-CoV-2 was generated by CPER as previously described.²⁰ In brief, the 9 fragments of SARS-CoV-2 and UTR linker for SARS-CoV-2 described above were prepared by PCR using PrimeSTAR GXL DNA polymerase (Takara Bio). To prepare recombinant SARS-CoV-2 expressing the genes of MA10, B.1.351.1, BA.1, XBB.1.5, NanoLuc, or Akaluc mutations, the respective F3, F4, F8, or F9-10 plasmids were used for CPER. To generate recombinant SARS-CoV-2, the CPER products (25 μ L) were transfected into HEK293-3P6C33 cells with Opti-MEM (Thermo Fisher Scientific) and TransIT-LT1 (Mirus Bio) according to the manufacturer's protocol. At 6 h post-transfection, the culture medium was replaced with DMEM containing 2% FBS, 1% PS, and doxycycline (1 μ g/mL) (InvivoGen). All viruses were stored at -80° C until use.

The infectious titers in culture supernatants were determined by quantifying the 50% tissue culture infectious dose (TCID₅₀).⁴⁹ Cell culture supernatants were used to inoculate naive VeroE6/TMPRSS2 cells in 96-well plates after 10-fold serial dilution with DMEM containing 1 mg/mL G418 (Nacalai Tesque) and 2% FBS, and the infectious titers were determined at 72 h post-infection (hpi).

Northern blotting

Total RNAs were extracted from cells infected with B.1.1 or B.1.1-Akaluc and were subjected to Northern blot analysis as previously described.²⁰ In brief, a digoxigenin (DIG)-labeled random-primed probe, corresponding to 28,999 to 29,573 of the SARS-CoV-2 genomes, was generated by using a DIG RNA Labeling kit (SP6/T7) (Sigma-Aldrich), and utilized to detect viral mRNAs. The RNAs were washed with the DIG luminescent detection kit (Sigma-Aldrich) and were visualized with CDP-Star Chemiluminescent Substrate (Sigma-Aldrich), according to the manufacturer's protocols. Bands were detected by WSE-6100 LuminoGraph I (Atto).

Quantitative RT-PCR

For quantification of viral RNA copies, total RNA was extracted from cells using a PureLink RNA Mini Kit (Thermo Fisher Scientific), and then first-strand cDNA synthesis and qRT-PCR were performed using One Step PrimeScript III RT-PCR Kit (Takara Bio) and QuantStudio 5 Real-Time PCR System (Thermo Fisher Scientific), respectively, according to the manufacturer's protocols. For quantification of viral RNA, primer sets detecting the region encoding part of the viral nucleocapsid phosphoprotein as reported in a previous study²² were used (See Table S1 for primer information). Fluorescent signals were determined by QuantStudio 5 Real-Time PCR System.

IHC

IHC was performed as previously described^{24–33} using an Autostainer Link 48 (Dako). The deparaffinized sections were exposed to EnVision FLEX target retrieval solution high pH (Agilent) for 20 min at 97°C for activation, and a mouse anti-SARS-CoV-2 N monoclonal antibody (clone 1035111, R&D Systems, dilution 1:400) was used as a primary antibody. The sections were sensitized using EnVision FLEX for 15 min and visualized by peroxidase-based enzymatic reaction with 3,3'-diaminobenzidine tetrahydrochloride (Dako) as substrate for 5 min. Images were incorporated as virtual slides by NDP.scan software v3.2.4 (Hamamatsu Photonics). The area of N-protein positivity was measured using Fiji software v2.2.0 (ImageJ).

QUANTIFICATION AND STATISTICAL ANALYSIS

All assays were performed in triplicate and independently repeated at least two times. Results were expressed as the means ± standard errors (SEM). Statistical significance was determined by the two-tailed Student's t test performed by GraphPad Prism (Software ver. 10.0.1). Significantly different values ($p < 0.05$) are indicated by an asterisk.